Journal of Neurochemistry

JOURNAL OF NEUROCHEMISTRY | 2015 | 132 | 342–353 doi: 10.1111/jnc.12981

ORIGINAL ARTICLE

Deletion of *Atf6α* impairs astroglial activation and enhances neuronal death following brain ischemia in mice

Akifumi Yoshikawa,* Tomoya Kamide,* Koji Hashida,†,‡ Hieu Minh Ta,† Yuki Inahata,† Mika Takarada-Iemata,†,‡ Tsuyoshi Hattori,† Kazutoshi Mori,‡,§ Ryosuke Takahashi,‡,¶ Tomohiro Matsuyama,** Yutaka Hayashi,* Yasuko Kitao†,‡ and Osamu Hori†,‡

*Department of Neurosurgery, Graduate School of Medical Sciences, Kanazawa University, Kanazawa City, Ishikawa, Japan

†Department of Neuroanatomy, Graduate School of Medical Sciences, Kanazawa University, Kanazawa City, Ishikawa, Japan

‡CREST (Core Research for Evolutionary Science and Technology), JST (Japan Science and Technology Agency), Tokyo, Japan

§Department of Biophysics, Graduate School of Science, Kyoto University, Kyoto City, Kyoto, Japan

¶Department of Neurology, Graduate School of Medicine, Kyoto University, Kyoto City, Kyoto, Japan

**Institute for Advanced Medical Sciences, Hyogo College of Medicine, Nishinomiya City, Hyogo, Japan

Abstract

To dissect the role of endoplasmic reticulum (ER) stress and unfolded protein response in brain ischemia, we investigated the relevance of activating transcription factor 6α (ATF6α), a master transcriptional factor in the unfolded protein response, after permanent middle cerebral artery occlusion (MCAO) in mice. Enhanced expression of glucose-regulated protein78, a downstream molecular chaperone of ATF6α, was observed in both neurons and glia in the peri-infarct region of wild-type mice after MCAO. Analysis using wild-type and *Atf6α*$^{-/-}$ mice revealed a larger infarct volume and increased cell death in the peri-ischemic region of *Atf6α*$^{-/-}$ mice 5 days after MCAO. These phenotypes in *Atf6α*$^{-/-}$ mice were associated with reduced levels of astroglial activation/glial scar formation, and a spread of tissue damage into the non-infarct area. Further analysis in mice and cultured astrocytes revealed that signal transducer and activator of transcription 3 (STAT3)-glial fibrillary acidic protein signaling were diminished in *Atf6α*$^{-/-}$ astrocytes. A chemical chaperone, 4-phenylbutyrate, restored STAT3-glial fibrillary acidic protein signaling, while ER stressors, such as tunicamycin and thapsigargin, almost completely abolished signaling in cultured astrocytes. Furthermore, ER stress-induced deactivation of STAT3 was mediated, at least in part, by the ER stress-responsive tyrosine phosphatase, TC-PTP/PTPN2. These results suggest that ER stress plays

Received August 20, 2014; revised manuscript received October 22, 2014; accepted October 22, 2014.

Address correspondence and reprint requests to Dr Osamu Hori, Department of Neuroanatomy, Kanazawa University Graduate School of Medical Sciences, 13-1 Takara-Machi, Kanazawa City, Ishikawa 920-8640, Japan. E-mail: osamuh3@staff.kanazawa-u.ac.jp

Abbreviations used: 3-NT, 3-nirotyrosine; 4-PBA, 4-phenylbutyrate; ATF4, activating transcription factor 4; ATF6α, activating transcription factor 6α; bpV, bisperoxovanadium; CHOP, C/EBP homologous protein; CNTF, ciliary neurotrophic factor; eIF2α, eukaryotic translation initiation factor 2; ERAD, ER-associated degradation; ER, endoplasmic reticulum; FSK, forskolin; GFAP, glial fibrillary acidic protein; GRP78, glucose-regulated protein78; Herp, homocysteine-inducible endoplasmic reticulum stress protein; HO-1, heme oxygenase 1; Ire1α, inositol-requiring enzyme 1α; LIF, leukemia inhibitory factor; MCAO, middle cerebral artery occlusion; ORP150, oxygen-regulated protein 150; PERK, protein kinase R (PKR)-like endoplasmic reticulum kinase; PTP, protein-tyrosine phosphatase; SOCS3, suppressor of cytokine signaling 3; ssDNA, single-stranded DNA; STAT3, signal transducer and activator of transcription 3; Tg, thapsigargin; Tm, tunicamycin; TTC, 2,3,5-triphenyl tetrazolium chloride; UPR, unfolded protein response.

critical roles in determining the level of astroglial activation and neuronal survival after brain ischemia.

Keywords: astrogliosis, brain ischemia, ER stress, neuronal death.
J. Neurochem. (2015) **132**, 342–353.

*Read the **Editorial Highlight** for this article on page 263.*

***Cover Image** for this issue: doi: 10.1111/jnc.12857.*

Stroke is a major cause of death and long-lasting disability in the most industrialized countries. Brain damage after cerebrovascular occlusion occurs through both flow-dependent and -independent mechanisms (Hossmann 2006; Amantea *et al.* 2009). A few minutes after the onset of ischemia, brain damage starts in the center of the ischemic region, or the ischemic core. At this stage, cell death is caused by acute energy failure and loss of ionic gradients associated with permanent and anoxic depolarization (Hossmann 1994; Dirnagl *et al.* 1999). A few hours later, the infarct area starts to expand into the bordering zone, penumbra, in which energy metabolism is partially preserved. Several pathways such as excitotoxicity, organelle dysfunction, and intracellular stress may be included in this step. Further brain damage is observed days to weeks after ischemia through vasogenic edema and inflammation. In contrast to the vulnerability of neurons, astrocytes, the most abundant glia in the brain, can survive and become activated after brain ischemia. Highly activated astrocytes form a barrier, the so-called glial scar, in the bordering zone that restricts inflammation and brain damage within the barrier (Sofroniew 2009).

Endoplasmic reticulum (ER) stress is characterized by the accumulation of unfolded proteins in the ER, and occurs in many pathophysiological conditions such as ischemia, impairment of protein modification, disturbance of Ca^{2+} homeostasis, and production of a large amount of proteins in the ER. Eukaryotic cells respond to ER stress by activating a set of pathways known as the unfolded protein response (UPR) (Walter and Ron 2011). In mammals, the UPR is transmitted through three types of sensor proteins: Protein kinase R (PKR)-like endoplasmic reticulum kinase (PERK), inositol-requiring enzyme 1α (Ire1α), and activating transcription factor 6α (ATF6α) (Walter and Ron 2011). Downstream molecules of Ire1α and ATF6α include molecular chaperones in the ER, such as glucose-regulated protein78 (GRP78), and oxygen-regulated protein 150 (ORP150), and ER-associated degradation molecules such as Derlins, and homocysteine-inducible endoplasmic reticulum stress protein (Herp). In contrast, PERK activation induces the phosphorylation of the alpha subunit of eukaryotic translation initiation factor 2 (eIF2α), which suppresses general protein synthesis to reduce protein loads into the ER, and activating transcription factor 4, which up-regulates the expression of heme oxygenase 1 and C/EBP homologous protein (CHOP) (Lewerenz and Maher 2009).

Ours and other groups have reported that brain ischemia causes ER stress and UPR activation both in human postmortem brains and rodent stroke models, the latter including both transient and permanent middle cerebral artery occlusion (MCAO) models (Tamatani *et al.* 2001; DeGracia and Montie 2004; Morimoto *et al.* 2007). We have also reported that both of GRP78 and OPR150 are up-regulated in cultured astrocytes exposed to hypoxia, and that over-expression of ORP150 in neurons increased neuronal survival after brain ischemia in mice (Tamatani *et al.* 2001). Compounds such as the chemical chaperone Sodium 4-phenylbutyrate (4-PBA) and UPR activator immunoglobulin heavy-chain binding protein (BIP) inducer X (BIX), both of which can ameliorate ER stress, have also been demonstrated to protect cortical neurons against brain ischemia in mice (Qi *et al.* 2004; Kudo *et al.* 2008). However, it is not yet clear whether the neuroprotective effect of the UPR against brain ischemia is mediated through cell-autonomous or non-cell-autonomous mechanisms.

To expand our understanding of the role of the UPR in brain ischemia, we initiated this study by estimating the status of UPR activation after permanent MCAO in wild-type mice. We then compared stroke size, neuronal death, glial activation/scar formation between wild-type and *Atf6α*$^{-/-}$ mice. Finally, we analyzed the impact of ER stress on astroglial activation using cultured astrocytes. Our data indicate that ER stress impedes astroglial activation/scar formation by suppressing signal transducer and activator of transcription 3 (STAT3)-Glial fibrillary acidic protein (GFAP) signaling, and enhances neuronal death and stroke volume after brain ischemia.

Materials and methods

Mice and induction of focal cerebral ischemia

All animal experiments were approved by the Animal Care and Use Committee of Kanazawa University. *Atf6α*$^{-/-}$ mice were generated as described previously (Yamamoto *et al.* 2007), and backcrossed to the C57BL/6 strain (Japan SLC, Inc, Hamamatsu, Shizuoka, Japan) more than eight times in the Institute of Laboratory Animals Graduate School of Medicine, Kyoto University, followed by the breeding in the Institute for experimental animals, Kanazawa University Advanced science research center. Wild-type and

Atf6α$^{-/-}$ male mice (aged 7–10 weeks and weighing 20–25 g) were used for the experiments. Permanent focal cerebral infarction was introduced by bipolar coagulation of the left MCA (middle cerebral artery) as described previously (Taguchi *et al.* 2004). Under isoflurane inhalation (2%), the left MCA was isolated, electrocauterized, and disconnected just distal to its crossing of the olfactory tract (distal M1 portion). Cerebral blood flow in the MCA area was monitored, and mice that showed decreased cerebral blood flow by approximately 75% immediately after ligation were used for our experiments (success rate of > 90%). Body temperature was maintained between 36.5°C and 37°C using a heat pad during the operation after MCAO. At the indicated times, brain samples were prepared for histological analyses, quantitative real time RT-PCR (qRT-PCR), and western blot as described below.

Measurement of infarct volume

Infarct volume was analyzed using 2,3,5-triphenyl tetrazolium chloride (TTC) staining (Koumura *et al.* 2009). Briefly, fresh brains were collected and sliced into five coronal sections, 2-mm thick. Sections were then stained with TTC (1%), and infarct areas were traced using Image J software (version 1.42, Wayne Rasband, National Institutes of Health, Bethesda, MD). Infarct volume between 2 adjacent sections was calculated by formula: $1/3 \times h(S1 + S2 + \sqrt{S1 \times S2})$, and whole infarct volume was obtained by totalizing each infarct volume (Huang *et al.* 2013).

Quantitative real time RT-PCR and conventional RT-PCR

Total RNA was extracted from the cerebral cortex (anterior area from Bregma −2.0 mm) of each mouse using RNeasy® Lipid Tissue Mini Kit (Qiagen, Valencia, CA, USA) or from cultured astrocytes using RNeasy® mini Kit (Qiagen). RT reactions containing 1 μg of total RNA were performed using PrimeScript™ (Takara, Otsu, Shiga, Japan). The individual cDNA was amplified with THUNDERBIRD™ SYBR qPCR® Mix (TOYOBO CO, LTD, Osaka, Japan) by using specific primers for *Hspa5*(GRP78), *Hyou1* (ORP150), *Ddit3*(CHOP), *Il6* (IL-6), *Lif*(LIF), *Tgfb1*(TGF-β), *Gfap* (GFAP), *Ptpn1*(PTP1B/PTPN1), *Ptpn2*(TC-PTP/PTPN2), and *Actb* (β-actin). The comparative Ct method was used for data analyses with MxPro 4.10 (Agilent Technologies, Santa Clara, CA, USA). Values for each gene were normalized to *Actb* expression levels. In some cases, the individual cDNA was amplified in a reaction mixture containing 1 unit of Taq DNA polymerase (Takara) and the isoform-specific primers for *Ptpn2*. Primer sequences for qPCR and conventional PCR are listed in Figure S1 and Figure S2, respectively.

Western blot and ELISA

Samples from the cerebral cortex (anterior area from Bregma −2.0 mm) or from the cultured astrocytes were solubilized in a buffer containing 1% NP40, 0.1% sodium dodecyl sulfate, and 0.2% deoxycholate. Solubilized samples were subjected to western blot with the following antibodies: GRP78 (StressGen, Victoria, British Columbia, Canada), GFAP (Dako, Glostrup, Denmark), Iba1 (Wako, Osaka City, Osaka, Japan), leukemia inhibitory factor (LIF) (Santa Cruz Biotechnology, Dallas, TX, USA), STAT3, p-STAT3 (Tyr705) (Cell Signaling Technology, Danvers, MA, USA), PTP1B/PTPN1 (Santa Cruz Biotechnology), TC-PTP/PTPN2 (Santa Cruz Biotechnology), SHP1/PTPN6 (Cell Signaling Technology), SHP2/PTPN11 (BD, Franklin Lakes, NJ, USA), HSP60 (StressGen), Lamin B (Santa Cruz Biotechnology), and β-actin (Sigma, St Louis, MO, USA). Primary antibody binding was visualized using the enhanced chemiluminescence system (GE Healthcare Bio-Sciences Corp., Piscataway, NJ, USA). IL-6 levels in brain samples were measured by ELISA (eBioscience, San Diego, CA, USA).

Histological and Immunohistochemical analyses

Brains were removed from mice after perfusion with 4% paraformaldehyde, and coronal sections (10-μm thick) were cut on a cryostat. Sections were processed for Fluoro-Jade C (FJC) staining (Millipore, Billerica, MA, USA) or for immunohistochemistry with following antibodies: GRP78 (StressGen), single-stranded DNA (ssDNA; Immuno-Biological Laboratories, Fujioka, Gumma, Japan), interleukin-6 (IL-6; R&D systems Inc., Minneapolis, MN, USA), NeuN (Millipore), GFAP (Dako), Iba1 (Wako), and 3-nitrotyrosine (Cayman Chemical Company, Ann Arbor, MI, USA). In some cases, the cell nuclei were visualized with DAPI (4',6-diamidino-2-phenylindole) (Sigma). Cy3-labeled-(Jackson ImmunoResearch Laboratories, West Grove, PA) and Alexa 488-labeled-IgG (Invitrogen, Carlsbad, CA) were used as secondary antibodies.

Cell culture

Astrocytes were isolated from cerebral cortex of 1- to 3-d-old neonatal mice following previously described methods with minor modifications (Hori *et al.* 1994; Kuwabara *et al.* 1996). Briefly, cerebral hemispheres were harvested from neonatal mice, and the meninges were carefully removed. Brain tissue was then digested at 37°C in HEPES-buffered saline containing Dispase II (2 mg/mL; Wako). Cells were collected by centrifugation and resuspended in minimum essential medium (Sigma) supplemented with 10% fetal bovine serum. After 10-days cultivation, microglial cells were removed by aspiration after shaking and the adherent cell population was collected and used for experiments. When the cultures achieved confluence, cells were incubated in serum-free medium for 8 h, and then treated with astroglial activators such as forskolin (FSK) (10 μM; Wako) and IL-6 (20 ng/mL; Wako), ER stressors such as tunicamycin (Tm) (2 μg/mL; Nacalai tesque, Kyoto, Japan) and thapsigargin (Tg) (0.3 μM; Nacalai tesque), or a chemical chaperone 4-PBA (1 mM; LKT Laboratories, Inc., St. Paul, MN, USA) in serum-free medium for the indicated times. In some cases, cells were also treated with protein-tyrosine phosphatase (PTP) inhibitors such as sodium orthovanadate (0.1–1 mM; Sigma), bisperoxovanadium (bpV) (10–50 μM, Enzo life sciences, Farmingdale, NY, USA), a histone deacetylase (HDAC) 1 inhibitor, TrichostatinA (TSA) (5 μM; Sigma), or Sirt1 inhibitor Ex527 (5 μM; AdooQ BioScience, Irvine, CA, USA).

Crude cell fractionation

Cultured astrocytes (10^7 cells) were homogenized using Dounce homogenizer in a buffer containing 0.25 M sucrose, 10 mM acetic acid, 10 mM triethanolamine, 1 mM EDTA, pH 7.4, and 1 mM phenylmethylsulfonyl fluoride. Samples were then subjected to the first centrifuge at 1000 *g* for 10 min (the nuclear fraction), the second centrifuge at 10 000 *g* for 10 min (mitochondrial fraction), and the centrifugation at 100 000 *g* for 60 min (the microsome and cytosolic fractions).

RNA interference

Specific siRNAs for *Ptpn1* and *Ptpn2*, *Ptpn6*, *Ptpn11*, and *Socs3* were obtained from Sigma, and negative control siRNA with a scrambled sequence was obtained from Invitrogen, Carlsbad, CA, USA. The target sequences of siRNAs are listed in Figure S3. Specific siRNAs or control siRNA were transfected into astrocytes using Lipofectamine RNAiMAX (Invitrogen) under the reverse transfection protocol according to the manufacturer's specification.

Image quantification and statistical analysis

Quantification of western blots and immunohistochemistry was performed using Image J. The number of ssDNA-positive cells, GFAP-positive cells, and Iba1-positive cells were counted in seven

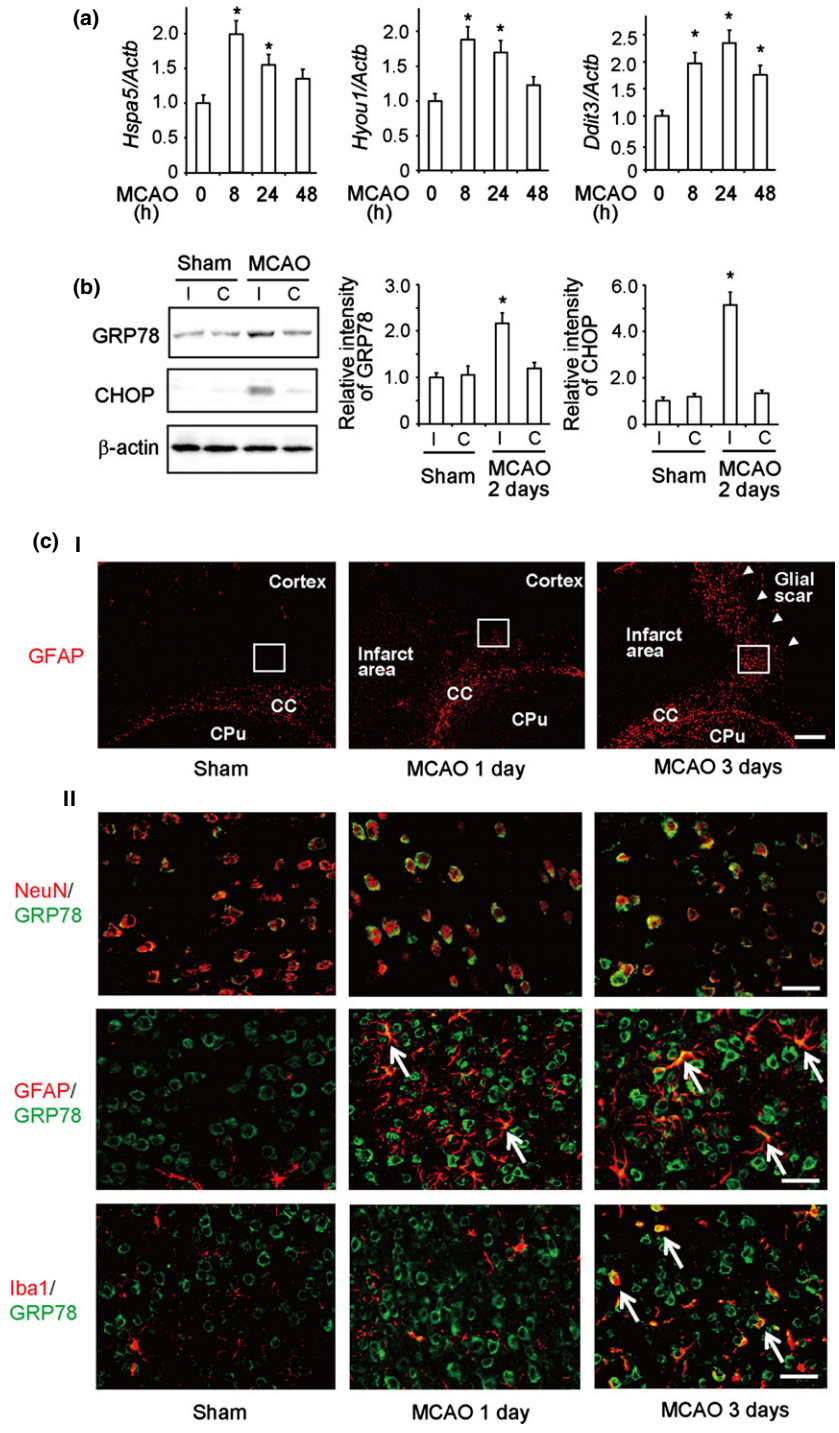

Fig. 1 Expression of the unfolded protein response (UPR)-target genes after middle cerebral artery occlusion (MCAO). (a) qRT-PCR. Wild-type (WT) mice were subjected to MCAO or sham operation, and total RNA (1 μg), extracted from the cerebral cortex, was analyzed by qRT-PCR. (b) Western blot. Wild-type (WT) mice were subjected to MCAO or sham operation, and protein (30 μg), extracted from the cerebral cortex, was subjected to western blot with the indicated antibodies. Values shown are the mean ± SD ($n = 4$). *$p < 0.05$, compared with mice with sham operation. (c) Immunohistochemistry. Brain sections from mice after MCAO or sham operation were analyzed by immunohistochemical analysis with the indicated antibodies. Rectangles in (c i) indicate the regions enlarged in (c ii). Arrows indicate co-localization of glucose-regulated protein78 (GRP78) with glial fibrillary acidic protein (GFAP) or Iba1. Scale bars = 200 μm (c i), 30 μm (c ii).

regions (total 0.07 mm^2) either in the infarct area (squares in dotted lines) or in the glial scar area (squares in solid lines) (Figure S1a). The relative sizes of GFAP-positive cells and Iba1-positive cells were calculated by dividing the GFAP-positive areas and Iba1-positive areas with the number of GFAP-positive cells and Iba1-positive cells, respectively. Statistical analyses were performed using Bonferroni/Dunn test following a one-way ANOVA or Student's *t*-test.

Results

Activation of the UPR after MCAO

We first analyzed the activating status of the UPR in our stroke model, in which the left MCA is permanently coagulated in mice (Taguchi *et al.* 2004). qRT-PCR analysis revealed enhanced mRNA expression in several UPR-target genes such as *Hspa5* and *Hyou1*, which encode molecular chaperones in the ER, GRP78, and ORP150, respectively, and *Ddit3*, which encodes a cell death-related molecule, CHOP, 8–24 h after MCAO (Fig. 1a). Western blot analysis confirmed the enhancement of GRP78 and CHOP protein levels 2 days after MCAO (Fig. 1b), suggesting that the effect of UPR activation may continue from the acute (hours) to subacute (days) phase after MCAO. Further immunohistochemical analysis revealed up-regulation of GRP78 expression in the border between the infarct and non-infarct area after MCAO (Fig. 1c ii). In the control condition (sham operation), a moderate level of expression of GRP78 was observed in NeuN-positive cortical neurons, but not in glial cells. In contrast, 1–3 days after MCAO, enhanced expression of GRP78 was observed both in neurons, GFAP-positive astrocytes, and Iba1-positive microglia/macrophages. In our model, UPR activation occurs earlier in astrocytes (24 h after MCAO) than in microglia/macrophages (72 h after MCAO).

Enhanced infarct size and cell death in *Atf6α*$^{-/-}$ mice after MCAO

To evaluate the neuroprotective role of the UPR in the MCAO model, we analyzed infarct volume (Fig. 2a) and cell death (Fig. 2b), using TTC staining and immunohistochemistry against ssDNA, respectively. Although there were no significant differences in TTC staining between wild-type and *Atf6α*$^{-/-}$ mice until 3 days after MCAO, the latter mice displayed a larger infarct volume than the former (15.5 ± 2.1 mm^3 and 23.2 ± 6.6 mm^3, respectively) 5 days after MCAO (Fig. 2a). Consistent with these results, ssDNA-positive apoptotic cells or FJC-positive neurodegenerative cells were restricted to the infarct area in wild-type mice 5 days after MCAO, while they were extended to the peri-infarct area in *Atf6α*$^{-/-}$ mice (Fig. 2b, Figure S1c). Importantly, glial scar formation in *Atf6α*$^{-/-}$ mice was less obvious than in wild-type mice (Fig. 2b). Further analysis revealed that the majority of ssDNA-positive cells in the border regions of *Atf6α*$^{-/-}$ mice were NeuN-positive neurons, while some of those are GFAP-positive astrocytes (Figure S1b).

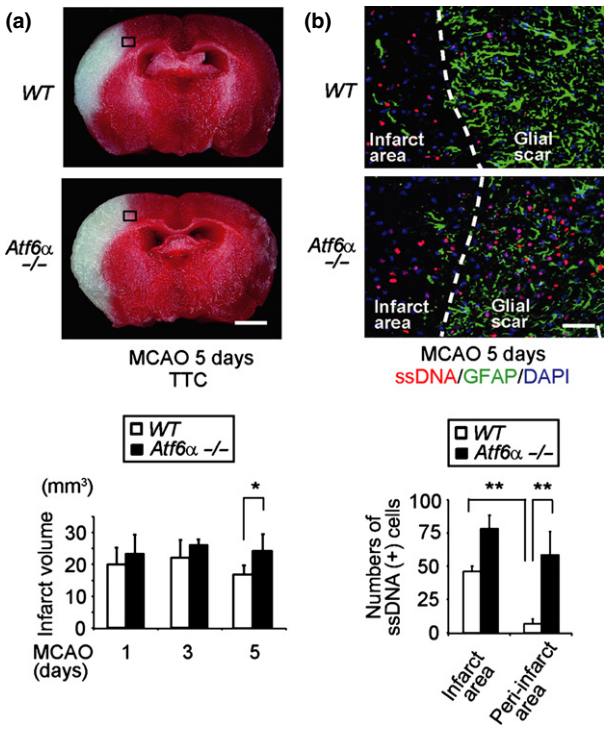

Fig. 2 Enhanced infarct volume and cell death in *Atf6α*$^{-/-}$ mice after middle cerebral artery occlusion (MCAO). (a) Infarct volume after MCAO. Wild-type and *Atf6α*$^{-/-}$ mice were subjected to MCAO or sham operation, and the forebrain section was analyzed by 2,3,5-triphenyltetrazolium (TTC) staining at the indicated times. Infarct volume was calculated and indicated in the graph. Values shown are the mean ± SD $*p < 0.05$, between wild-type and *Atf6α*$^{-/-}$ brains ($n = 5$). B, Cell death after MCAO. Wild-type and *Atf6α*$^{-/-}$ mice were subjected to MCAO or sham operation as above, and they were perfused with 4% paraformaldehyde at the indicated times. The forebrain section was prepared, and was analyzed by immunohistochemistry using the indicated antibodies. The number of ssDNA-positive cells was counted and are indicated in the graph. Values shown are the mean ± SD. $*p < 0.05$, $**p < 0.01$, significantly different between 2 conditions ($n = 4$). Scale bars = 1 mm (a), 20 μm (b).

Impaired astroglial activation in *Atf6α*$^{-/-}$ mice after MCAO

As the UPR was activated both in neurons and glial cells (Fig. 1c ii), and glial scar formation in *Atf6α*$^{-/-}$ mice was less obvious than in wild-type mice (Fig. 2b), we hypothesized that glial activation, which could strongly influence neuronal survival/death, may be affected by deletion of *Atf6α* gene. Immunohistochemical analysis revealed that hypertrophic, GFAP-positive astrocytes were accumulated at the border between infarct and non-infarct area 3 days after MCAO in wild-type mice. In contrast, this astroglial accumulation was less observed in the same condition in *Atf6α*$^{-/-}$ mice (Fig. 3a i). Interestingly, the size of each astrocyte was smaller in *Atf6α*$^{-/-}$ mice, while the number was not significantly different between wild-type and *Atf6α*$^{-/-}$ mice (Fig. 3a ii), suggesting that deletion of *Atf6α* gene

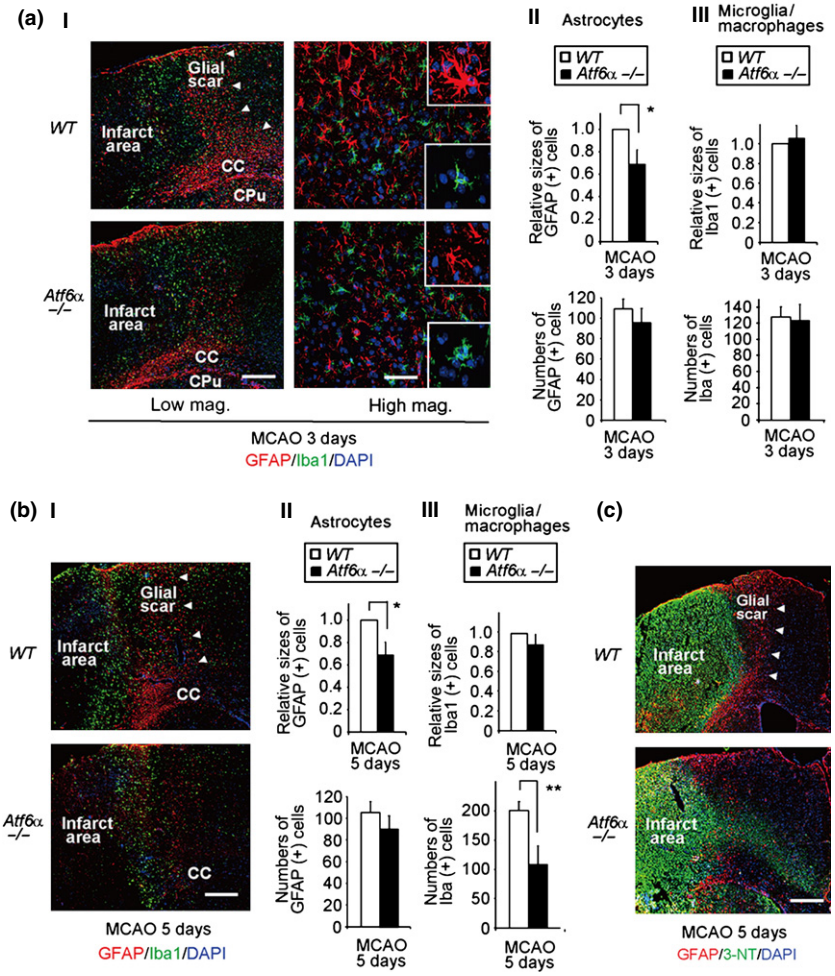

Fig. 3 Impaired astroglial activation in *Atf6α*$^{-/-}$ mice after middle cerebral artery occlusion (MCAO). (a and b) Astroglial and microglial activation 3 days (a) and 5 days (b) after MCAO. Brain sections from wild-type and *Atf6α*$^{-/-}$ mice after MCAO were analyzed by immunohistochemistry with the indicated antibodies. Nuclei were stained with DAPI. The relative sizes of activated astrocytes (a ii and b ii) and microglia/macrophages (a iii and b iii) were calculated and are indicated in the upper graphs. The relative sizes in wild-type mice were designated as one. The numbers of activated astrocytes (a ii and b ii) and microglia/macrophages (a iii and b iii) were counted and are indicated in the lower graphs. Values shown are the mean ± SD. *$p < 0.05$, **$p < 0.01$, significantly different between 2 conditions ($n = 4$). (c) Immunohisitochemical detection of 3-NT-pisitive area after MCAO. Brain sections from wild-type and *Atf6α*$^{-/-}$ mice after MCAO were analyzed by immunohistochemistry with the indicated antibodies. Nuclei were stained with DAPI. Scale bars = 200 μm (a i, low mag., b i and c), 40 μm (a i, high mag.).

may impair hypertrophic change, rather than proliferation of astrocytes after MCAO. In this period, the size and number of Iba1-positive microglia was not significantly changed in both genotypes (Fig. 3a iii). Five days after MCAO, the size of each astrocyte was still smaller in *Atf6α*$^{-/-}$ mice, when compared with wild-type mice (Fig. 3b i, ii). In addition, the number of Iba1-positive microglia/macrophages was somewhat lower in *Atf6α*$^{-/-}$ mice when compared with wild-type mice (Fig. 3b i, iii). Consistent with the lower levels of astroglial activation/glial scar formation, the 3-nirotyrosine (3-NT)-positive area, which is a marker of oxidative stress and tissue injury, was expanded into non-infarct areas in *Atf6α*$^{-/-}$ mice 5 days after MCAO (Fig. 3c).

To confirm the reduced levels of astroglial activation in *Atf6α*$^{-/-}$ mice after MCAO, western blot analysis was performed using samples of ipsilateral (I) and contralateral (C) cortex in both genotypes. As early as 2 days after MCAO, the expression of marker proteins for astroglial activation such as phosphorylated STAT3 (p-STAT3) and GFAP (Okada *et al.* 2006; Herrmann *et al.* 2008) was lower in the *Atf6α*$^{-/-}$ ipsilateral cortex when compared with wild-type ipsilateral cortex, and this lasted until 5 days after MCAO (Fig. 4a–c). The expression of GRP78 was lower in both of ipsilateral and contralateral cortex of *Atf6α*$^{-/-}$ mice when compared with wild-type mice between 2 and 5 days after MCAO (Fig. 4a–c). In contrast, the expression of CHOP, which is mainly regulated by PERK pathway, was not different between wild-type and *Atf6α*$^{-/-}$ mice 2 days after MCAO (Figure S2a). The expression of Iba1, a common marker of microglia/macrophages, was not significantly different between two genotypes until 3 days after MCAO, and expression became lower in the *Atf6α*$^{-/-}$ ipsilateral cortex 5 days after MCAO (Fig. 4a–c), which was consistent with the result of immunohistochemistry result (Fig. 3b i, iii). These results collectively suggest that deletion of the *Atf6α* gene affects astroglial activation at relatively early stages following ischemic injury.

Reduced STAT3 signaling in *Atf6α*$^{-/-}$ astrocytes after MCAO

Several cytokines and growth factors that are secreted from damaged neurons or other cells in the brain can induce astroglial activation, predominantly through the STAT3-GFAP pathway (Okada *et al.* 2006; Herrmann *et al.* 2008). Therefore, we examined the expression level of these genes

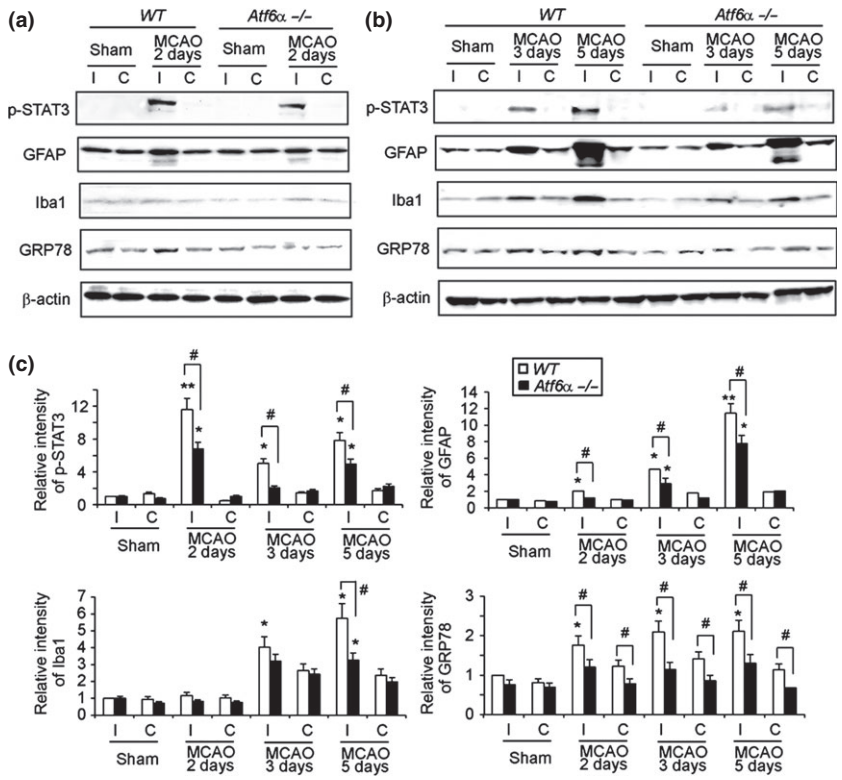

Fig. 4 Expressions of glial markers after middle cerebral artery occlusion (MCAO). (a and b) Wild-type and *Atf6*$\alpha^{-/-}$ mice were subjected to MCAO or sham operation, and protein was extracted from the cerebral cortex either 2 days (a), 3 days, or 5 days (b) after MCAO. Samples were analyzed by western blot using the indicated antibodies. (c) Relative band intensity is shown in the graphs. The intensities in the ipsilateral cortex of wild-type sham-operated mice are designated as one. Values shown are the mean ± SD ($n = 4$). $^{*}p < 0.05$, $^{**}p < 0.01$, when compared with mice after sham operation. $^{\#}p < 0.05$, compared between wild-type and ATF6$\alpha^{-/-}$ brains.

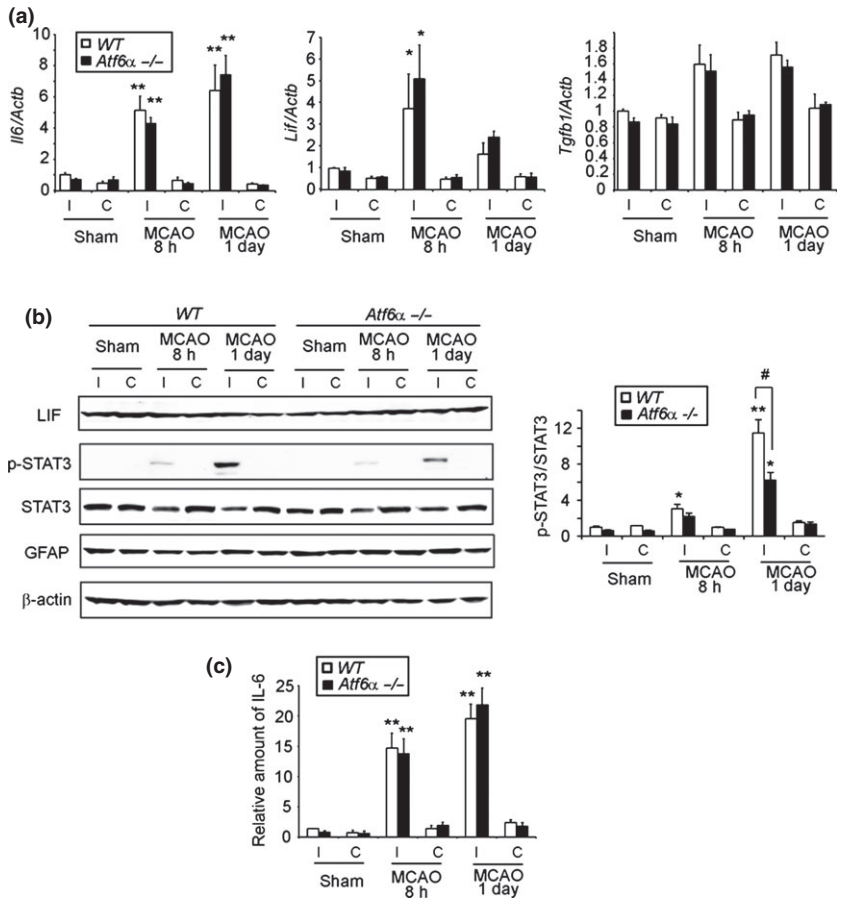

Fig. 5 Activating status of astrocytes after middle cerebral artery occlusion (MCAO). Wild-type and *Atf6*$\alpha^{-/-}$ mice were subjected to MCAO or sham operation, and total RNA (1 μg) or protein, extracted from the cerebral cortex, was analyzed by qRT-PCR (a), western blot (b) or ELISA (c). In (b) the ratio of p-STAT3 versus total signal transducer and activator of transcription 3 (STAT3) is shown in the graph. The intensities in the ipsilateral cortex of wild-type sham-operated mice were designated as one. Values shown are the mean ± SD ($n = 4$). $^{*}p < 0.05$, $^{**}p < 0.01$, when compared with mice after sham operation. $^{\#}p < 0.05$, compared between wild-type and *Atf6*$\alpha^{-/-}$ brains.

in wild-type and *Atf6α*$^{-/-}$ mice. qRT-PCR analysis revealed that mRNA expression of cytokines, such as LIF (*Lif*) and IL-6 (*Il6*), was significantly enhanced after MCAO, while there was no difference between two genotypes (Fig. 5a). The expression of (transforming growth factor) TGFβ (*Tgfb1*) (Fig. 5a) or ciliary neurotrophic factor (CNTF) (*Cntf*) (data not shown) was not significantly enhanced after MCAO in either genotype. Consistent with these results, western blot and ELISA analysis revealed that there was no significant difference in the expression of LIF (Fig. 5b) or IL-6 (Fig. 5c) between wild-type and *Atf6α*$^{-/-}$ mice after MCAO. Further immunohistochemical analysis revealed that IL-6 was mainly produced in damaged neurons in these periods (Figure S2b). In contrast, the activating status of STAT3, which was determined by the level of p-STAT3, was lower in *Atf6α*$^{-/-}$ mice when compared with wild-type mice 1 day after MCAO (Fig. 5b), suggesting that the reduced level of astroglial activation in *Atf6α*$^{-/-}$ mice is associated with impaired signaling pathways in astrocytes.

Impaired STAT3-GFAP signaling in *Atf6α*$^{-/-}$ and ER stress-exposed astrocytes

To confirm the impairment of activation-related signaling pathways in *Atf6α*$^{-/-}$ astrocytes, we employed cultured astrocytes isolated from the cerebral cortices of neonatal wild-type and *Atf6α*$^{-/-}$ mice. After serum deprivation for 8 h, cells were stimulated with FSK or IL-6 for 30 min. Western blot analysis revealed that p-STAT3 was detected in the normal condition in wild-type astrocytes, consistent with a previous report showing that cultured astrocytes are at least partially activated without stimulation (Zamanian *et al.* 2012). p-STAT3 expression was enhanced to 140% and 170% by FSK and IL-6 treatment, respectively (Fig. 6a, white bars). In contrast, the level of p-STAT3 in *Atf6α*$^{-/-}$ astrocytes was significantly lower in both of control and stimulated conditions (approximately 40, 65, and 65% when compared with wild-type astrocytes in normal, FSK-stimulated, and IL-6-stimulated conditions, respectively) (Fig. 6a, black bars). Consistent with these results, the expression of *Gfap* was lower in *Atf6α*$^{-/-}$ astrocytes when compared with wild-type astrocytes (Fig. 6b). To analyze the role of ER stress in the reduced activation of the STAT3/GFAP pathway in *Atf6α*$^{-/-}$ astrocytes, cells were treated with the chemical chaperone 4-PBA for 8 or16 h. 4-PBA is often used for attenuating ER stress (Qi *et al.* 2004; Kimura *et al.* 2012). Western blot and qRT-PCR analyses revealed that 4-PBA enhanced the level of p-STAT3 and *Gfap* in both wild-type and *Atf6α*$^{-/-}$ astrocytes in a dose dependent manner (Fig. 6c and d). In contrast, when wild-type astrocytes were treated with common ER stressors, such as Tm and Tg, the

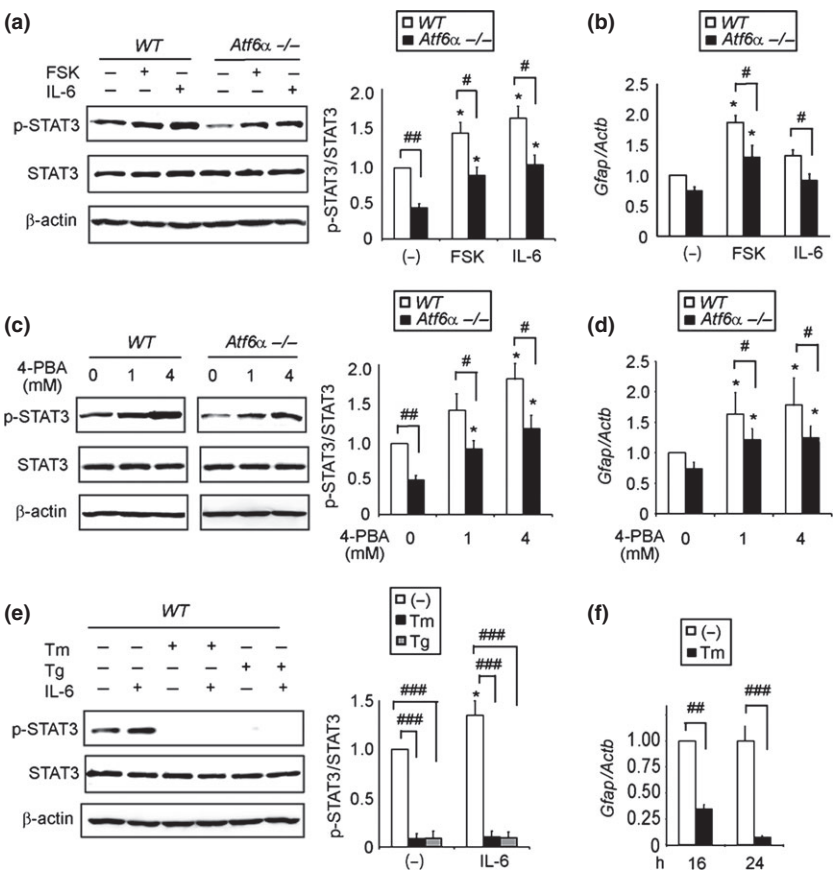

Fig. 6 Impaired signal transducer and activator of transcription 3 (STAT3)-glial fibrillary acidic protein (GFAP) signaling in ATF6α$^{-/-}$ and endoplasmic reticulum (ER) stress-exposed astrocytes (a and b) Cultured astrocytes, isolated from cerebral cortices of neonatal wild-type and ATF6α$^{-/-}$ mice, were stimulated with the indicated reagents for either 30 min (a) or 8 h (b) in serum-free conditions, and analyzed by western blot (a) or by qRT-PCR (b). (c and d) Cultured astrocytes were incubated with 4-phenylbutyrate (4-PBA) or medium alone for 8 h in serum-free conditions, and analyzed by western blot (c) or by qRT-PCR (d). Values shown are the mean ± SD ($n = 4$). $^{*}p < 0.05$, when compared with cells without stimulation. $^{\#}p < 0.05$, $^{\#\#}p < 0.01$, compared between wild-type and ATF6α$^{-/-}$ astrocytes. (e and f) Cultured astrocytes were incubated with ER stressors or medium alone for 8 h (e) or for the indicated times (f) in serum-free conditions, and analyzed by western blot (e) or by qRT-PCR (f), respectively. Values shown are the mean ± SD ($n = 4$). $^{\#}p < 0.05$, $^{\#\#}p < 0.01$, $^{\#\#\#}p < 0.005$, when compared between the indicated conditions.

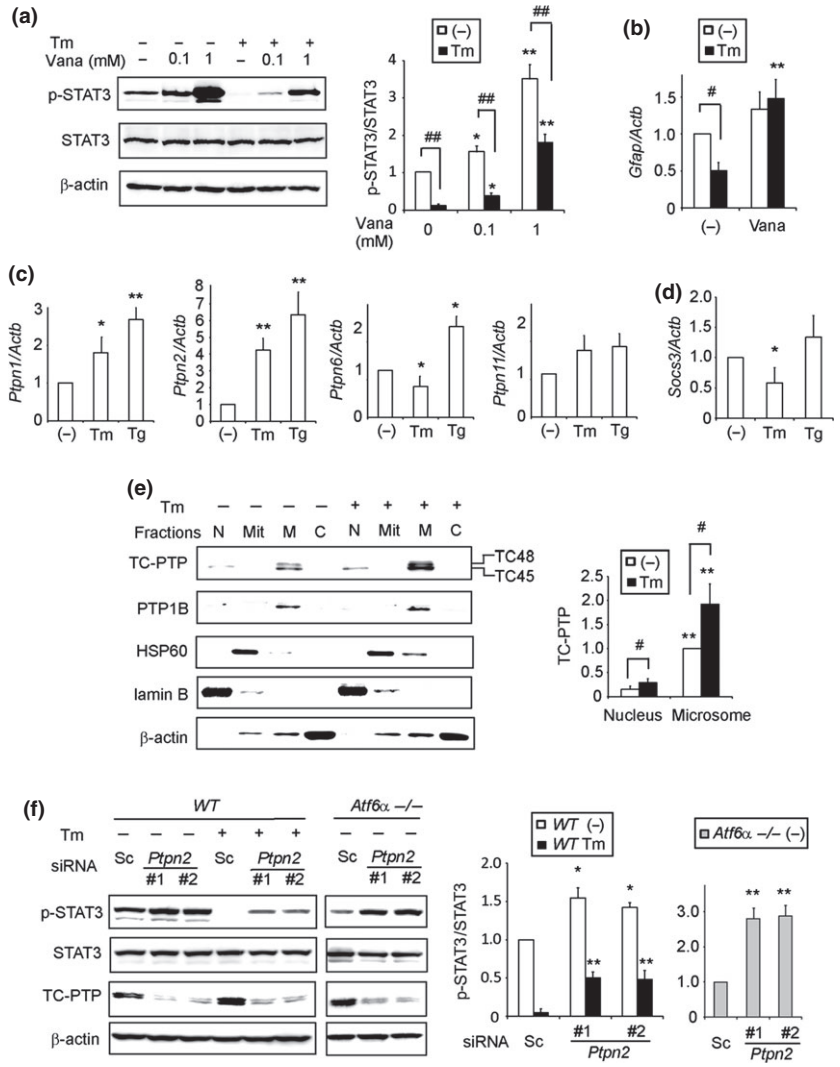

Fig. 7 The effect of protein-tyrosine phosphatases on signal transducer and activator of transcription 3 (STAT3)-glial fibrillary acidic protein (GFAP) signaling in astrocytes. (a and b) Cultured astrocytes, isolated from cerebral cortexes of neonatal wild-type mice, were stimulated with Orthovanadate (Vana) in the presence or absence of tunicamycin (Tm) for either 8 h (a) or 16 h (b) in serum-free conditions, and analyzed by western blot (a) or by qRT-PCR (b). (c and d) Cultured astrocytes were incubated with endoplasmic reticulum (ER) stressors or medium alone for 8 h in serum-free conditions, and analyzed by qRT-PCR. (e) Crude cell fractionation. Cultured astrocytes were incubated with tunicamycin or medium alone for 8 h in serum-free conditions, and subjected to crude cell fractionation as described in the text. Samples from each fraction were analyzed by western blot. N, nucleus; Mit, mitochondria; M, microsome; C, sytosol. Values shown are the mean ± SD ($n = 4$). $^{*}p < 0.05$, $^{**}p < 0.05$, when compared with cells without stimulation. $^{\#}p < 0.05$, when compared between the indicated conditions. (f) Gene silencing in wild-type and *Atf6α*$^{-/-}$ astrocytes. Cultured astrocytes were transfected with either scrambled siRNA (Sc) or *Prpn2* siRNAs (*Ptpn2* #1, #2), and cultured for 2 days. Cells were then incubated with serum-free condition for 8 h, and subjected with western blot.

expression of p-STAT3 and *Gfap* was almost completely abolished (Fig. 6e and f). These results suggest that ER stress strongly suppresses STAT3-mediated astroglial activation.

Involvement of TC-PTP in the impaired STAT3-GFAP signaling in ER stress-exposed astrocytes

To dissect the mechanism underlying the ER stress-mediated impairment of STAT3-GFAP signaling in astrocytes, we treated wild-type astrocytes with several compounds which are known to regulate p-STAT3 expression (Kimura *et al.* 2012), in the presence or absence of Tm. Orthovanadate (Vana), a broad PTP inhibitor, dose-dependently enhanced expression of p-STAT3 in both normal and ER stress conditions (Fig. 7a). Similarly, bisperoxovanadium (bpV), a more potent PTP inhibitor, strongly enhanced expression of p-STAT3 in the presence of Tm (Figure S2a). In contrast, the HDAC 1 inhibitor, TSA, or Sirt1 inhibitor, Ex527, did not enhance expression of p-STAT3 in the same condition (Figure S2a). These results suggest that PTPs may play an important role in the regulation of STAT3 signaling in astrocytes. Consistent with these results, the expression of *Gfap* was enhanced by Vana under ER stress condition (Fig. 7b).

Previous reports have demonstrated that several PTPs, such as PTP1B/PTPN1, TC-PTP/PTPN2, SHP1/PTPN6, and SHP2/PTPN11, are expressed in astrocytes and/or C6 astroglioma (Faure and Posner 1993; Servidei *et al.* 1998; Horvat *et al.* 2001). Therefore, we hypothesized that PTPs may be critical for regulating STAT3-GFAP signaling in astrocytes both in normal and under ER stress. qRT-PCR revealed that *Ptpn2*, and to a lesser degree *Ptpn1*, were up-regulated by both Tm and Tg (Fig. 7c), suggesting a possible association with these genes and ER stress. As there are two protein isoforms, TC45 and TC48, in TC-PTP/PTPN2, we analyzed whether both isoforms respond to ER stress. RT-PCR with isoform-specific primers revealed that expressions of both TC45 and TC48 are enhanced by ER stressors, although the expression level may be higher in TC45 (Figure

S2). In contrast, expression of *Ptpn6* was slightly enhanced by Tg, but suppressed by Tm (Fig. 7e), and that of *Ptpn11* was not enhanced by Tm or Tg (Fig. 7c). Suppressor of cytokine signaling 3 (SOCS3) is also a potent endogenous regulator of STAT3; therefore, we measured expression of *Socs3* in cultured astrocytes. qRT-PCR revealed that *Socs3* was not induced by Tm or Tg in our model, but its expression level was reduced by Tm (Fig. 7d). At protein levels, western blot analysis using samples after crude cell fractionation revealed that TC-PTP/PTPN2 was located in the microsome fraction and, to a lesser extent, in the nucleus fraction (Fig. 7e). The expression of TC-PTP/PTPN2 was enhanced by Tm in both fractions (Fig. 7e). In contrast, PTP1B/PTPN1 was located exclusively in the microsome fraction, and its expression did not changed by Tm (Fig. 7e).

To confirm the suppressive effect of PTPs on the STAT3 activation, gene-silencing experiments were performed using wild-type and *Atf6*$\alpha^{-/-}$ astrocytes. Two independent siRNAs per gene were introduced, and cell lysates were analyzed by western blot (Fig. 7f). Knockdown of *Ptpn2* significantly enhanced expression of p-STAT3 in both normal and ER stress conditions (Fig. 7f). However, knockdown of other *Ptps* (Figure S2b) or *Socs3* (data not shown) failed to enhance the expression of p-STAT3. In these gene-silencing experiments, the expression of each gene was reduced to less than 20% of control levels (Fig. 7f and Figure S2b).

Discussion

In this study, we have demonstrated that deletion of *Atf6*α gene increases infarct volume and neuronal death in the peri-infarct region after MCAO in mice. These phenotypes in *Atf6*$\alpha^{-/-}$ mice were associated with reduced astroglial activation/glial scar formation and a spread of tissue damage into the non-infarct region. Further analysis revealed that ER stress shut down the STAT3-GFAP signaling, one of the most critical pathways for astroglial activation, at least in part, through the ER stress-responsive tyrosine phosphatase, TC-PTP.

Astrocytes play important roles in various neuropathological situations, including acute brain insults such as stroke and trauma. In these conditions, astrocytes undergo hypertrophy and up-regulate intermediate filaments such as GFAP and vimentin, and this is referred to as reactive astrogliosis or astroglial activation. Although reactive astrogliosis has both detrimental and beneficial aspects, recent studies have emphasized its neuroprotective role through the regulation of inflammation and restoration of brain tissue (Okada *et al.* 2006; Herrmann *et al.* 2008; Li *et al.* 2008). Our results also demonstrated that attenuated astrogliosis/glial scar formation, caused by deletion of *Atf6*$\alpha^{-/-}$, lead to a spreading of tissue damage and cell death 5 days after MCAO (Figs 2b and 3c). In contrast to the phenotypes in astrocytes, altered microglia/macrophage phenotypes in *Atf6*$\alpha^{-/-}$ mice were not seen until 3 days after MCAO, while they became significant 5 days after MCAO. There were lower numbers of Iba1-positive cells in the border between infarct and non-infarct area in *Atf6*$\alpha^{-/-}$ mice (Fig. 3b i, iii). These phenotypes in *Atf6*$\alpha^{-/-}$ microglia/macrophages may be attributed to a direct effect of *Atf6*α deletion on microglia/macrophages, or an indirect effect through a reduced level of astrogliosis. Further studies using conditional *Atf6*α knockout mice will provide detailed mechanisms regarding the phenotypes found in *Atf6*$\alpha^{-/-}$ microglia/macrophages.

We have previously reported that neuron-specific overexpression of ORP150, a downstream molecule of ATF6α, protected against brain ischemia through mechanisms including Ca^{2+} homeostasis and production of neurotrophic factors (Kitao *et al.* 2001; Tamatani *et al.* 2001). In contrast, the current study emphasizes the neuroprotective role of ATF6α through a non-cell-autonomous mechanism, astroglial activation/scar formation. These discrepancies could be attributed to different types of genetic modification in mice and different models used to induce brain ischemia. In the previous report, we used neuron-specific ORP150 Tg mice or *Hyou1*$^{+/-}$ mice, because *Hyou1*$^{-/-}$ mice are embryonic lethal (Kitao *et al.* 2001), while in this study, we have used *Atf6*$\alpha^{-/-}$ mice as they have normal development and can be used for MCAO. Furthermore, in the previous work, we estimated stroke volume and neuronal survival 24 h after MCAO, when glial scar was not yet formed, while, in this study, we did measure up to 5 days after MCAO. The basal expression of GRP78 protein in *Atf6*$\alpha^{-/-}$ mice was not different from that in wild-type mice (Fig. 4). This may be because of the compensatory function of other UPR pathways such as ATF6β and Ire1 (Yamamoto *et al.* 2007).

Among intracellular signaling pathways, STAT3 pathway is among the most critical for inducing astrogliosis (Okada *et al.* 2006; Li *et al.* 2008). In response to extracellular signals such as IL-6, CNTF, and LIF, STAT3 is phosphorylated and translocates to the nucleus, where it promotes transcription of downstream genes including *Gfap* (Yeo *et al.* 2013). In the current study, the expression of IL-6, LIF, or CNTF was not altered between wild-type and *Atf6*$\alpha^{-/-}$ mice in either control or ischemic conditions, while the level of p-STAT3, phosphorylated STAT3, was lower in *Atf6*$\alpha^{-/-}$ mice when compared with wild-type mice after MCAO (Fig. 5b). Similarly, the level of p-STAT3 was lower in *Atf6*$\alpha^{-/-}$ astrocytes than wild-type astrocytes *in vitro* (Fig. 6a). Treatment of cells with a chemical chaperone, 4-PBA, or with ER stressors, such as Tm and Tg, increased and decreased the levels of p-STAT3 and *Gfap*, respectively (Fig. 6c–f). These results suggest that enhanced level of ER stress in the basal *Atf6*$\alpha^{-/-}$ astrocytes suppresses STAT3-GFAP signaling.

Recent reports have demonstrated that ER stress regulates STAT3 signaling through different mechanisms, including PTP1B-dependent tyrosine dephosphorylation and HDAC-

dependent deacetylation (Kimura *et al.* 2012). In our model, tyrosine phosphatase inhibitors such as orthovanadate and bpV, but not a HDAC inhibitor, TSA, or Sirt1 inhibitor, Ex527, enhanced levels of p-STAT3, and *Gfap* in both of normal and Tm-treated conditions (Fig. 7a and b). There are several PTPs expressed in astrocytes and/or C6 astroglioma (Navis *et al.* 2010), and some, such as PTP1B/PTPN1 and TC-PTP/PTPN2, are located, at least partly, in the ER. In our model, *Ptpn2* had the strongest response to ER stress (Fig. 7c and d), and knockdown of *Ptpn2*, but not other genes, enhanced the level of p-STAT3 in all conditions tested (Fig. 7f).

TC-PTP/PTPN2 is a ubiquitously expressed, non-receptor-type PTP that has a similar structure to PTP1B/PTPN1 (Navis *et al.* 2010). Two protein isoforms, TC45 and TC48, are generated by alternative splicing (Mosinger *et al.* 1992). TC45 is located in the nucleus, and regulates diverse signaling molecules including STAT3 (Muppirala *et al.* 2013). TC48, in contrast, is anchored to the ER membrane using its hydrophobic carboxyl terminus, and may function in a secretory pathway (Muppirala *et al.* 2013). Our results indicate that both of TC45 and TC48 are expressed in astrocytes, and are up-regulated by ER stress, although the expression level may be higher in TC45 (Figure S2), as previously described (Mosinger *et al.* 1992). Further crude cell fractionation analysis revealed that not only T48 but also the majority of T45 was observed in the microsome fraction in our system (Fig. 7e), suggesting that TC45 may be recruited to some type of membrane in the secretory pathway. It has been reported that the expression of PTP1B/PTPN1, but not TC-PTP/PTPN2, is increased by ER stress in pancreatic β cells (Beamer *et al.* 2006). The discrepancy with our results may be attributed to the duration of ER stress (days vs. hours) and the cell types (pancreatic β cells vs. astrocytes). At this moment, we do not exclude the possibility that other PTPs, such as SHP-1, may also play important roles in regulating astroglial and microglial activation, as previously described (Hashida *et al.* 2012). Further studies will be required to clarify the roles of TC-PTP and other PTPs in diverse neuropathological situations, including Parkinson's disease, in which we also observed reduced astroglial activation in *Atf6α*$^{-/-}$ mice (Cheng *et al.* 2002). It will also be intriguing to test the effect of PTP inhibitors on astroglial activation and neuroprotection *in vivo*.

It has been reported that both PTP1B and TC-PTP play critical roles in the insulin and/or leptin resistance through the suppression of STAT3 pathway (Zabolotny *et al.* 2002; Fukushima *et al.* 2010). As astrocytes also contribute to energy homeostasis in the brain both in normal and pathological conditions, it would be important to find the role of these PTPs in the insulin/leptin signaling in astrocytes. Analysis of PTPs in astrocytes will provide new insight into the research of stress response and neuronal death in the central nervous system.

Acknowledgments and conflict of interest disclosure

We thank Mr Takashi Tamatani for technical assistance. We are also grateful to Dr Hideaki Hara (Gifu Pharmaceutical University) for valuable comments regarding MCAO. This work was supported by a Grant-in Aid for Scientific Research (24500419) from the Ministry of Education, Science, Technology, Sports and Culture of Japan. The authors have no conflicts of interest to declare.

All experiments were conducted in compliance with the ARRIVE guidelines.

Supporting information

Additional supporting information may be found in the online version of this article at the publisher's web-site:

Figure S1. (a) The areas used to count ssDNA-, GFAP-, and Iba1-positive cells after MCAO.

Figure S2. (a) Expression of CHOP after MCAO. Wild-type and *Atf6α-/-* mice were subjected to MCAO or sham operation, and protein was extracted from the cerebral cortex after MCAO.

Figure S3. The effect of protein-tyrosine phosphatases on p-STAT3 expression in astrocytes.

References

Amantea D., Nappi G., Bernardi G., Bagetta G. and Corasaniti M. T. (2009) Post-ischemic brain damage: pathophysiology and role of inflammatory mediators. *FEBS J.* **276**, 13–26.

Beamer C. A., Brooks D. M. and Lurie D. I. (2006) Motheaten (me/me) mice deficient in SHP-1 are less susceptible to focal cerebral ischemia. *J. Neurosci. Res.* **83**, 1220–1230.

Cheng A., Uetani N., Simoncic P. D., Chaubey V. P., Lee-Loy A., McGlade C. J., Kennedy B. P. and Tremblay M. L. (2002) Attenuation of leptin action and regulation of obesity by protein tyrosine phosphatase 1B. *Dev. Cell* **2**, 497–503.

DeGracia D. J. and Montie H. L. (2004) Cerebral ischemia and the unfolded protein response. *J. Neurochem.* **91**, 1–8.

Dirnagl U., Iadecol C. and Moskowitz M. A. (1999) Pathobiology of ischaemic stroke: an integrated view. *Trends Neurosci.* **22**, 391–397.

Faure R. and Posner B. I. (1993) Differential intracellular compartmentalization of phosphotyrosine phosphatases in a glial cell line: TC-PTP versus PTP-1B. *Glia* **9**, 311–314.

Fukushima A., Loh K., Galic S., Fam B., Shields B., Wiede F., Tremblay M. L., Watt M. J., Andrikopoulos S. and Tiganis T. (2010) T-cell protein tyrosine phosphatase attenuates STAT3 and insulin signaling in the liver to regulate gluconeogenesis. *Diabetes* **59**, 1906–1914.

Hashida K., Kitao Y., Sudo H., Awa Y., Maeda S., Mori K., Takahashi R., Iinuma M. and Hori O. (2012) ATF6alpha promotes astroglial activation and neuronal survival in a chronic mouse model of Parkinson's disease. *PLoS ONE* **7**, e47950.

Herrmann J. E., Imura T., Song B., Qi J., Ao Y., Nguyen T. K., Korsak R. A., Takeda K., Akira S. and Sofroniew M. V. (2008) STAT3 is

a critical regulator of astrogliosis and scar formation after spinal cord injury. *J. Neurosci.* **28**, 7231–7543.

Hori O., Matsumoto M., Maeda Y., Ueda H., Ohtsuki T., Stern D. M., Kinoshita T., Ogawa S. and Kamada T. (1994) Metabolic and biosynthetic alterations in cultured astrocytes exposed to hypoxia/reoxygenation. *J. Neurochem.* **62**, 1489–1495.

Horvat A., Schwaiger F., Hager G., Brocker F., Streif R., Knyazev P., Ullrich A. and Kreutzberg G. W. (2001) A novel role for protein tyrosine phosphatase shp1 in controlling glial activation in the normal and injured nervous system. *J. Neurosci.* **21**, 865–874.

Hossmann K. A. (1994) Viability thresholds and the penumbra of focal ischemia. *Ann. Neurol.* **36**, 557–565.

Hossmann K. A. (2006) Pathophysiology and therapy of experimental stroke. *Cell. Mol. Neurobiol.* **26**, 1057–1083.

Huang J., Li Y., Tang Y., Tang G., Yang G. Y. and Wang Y. (2013) CXCR4 antagonist AMD3100 protects blood-brain barrier integrity and reduces inflammatory response after focal ischemia in mice. *Stroke* **44**, 190–197.

Kimura K., Yamada T., Matsumoto M. *et al.* (2012) Endoplasmic reticulum stress inhibits STAT3-dependent suppression of hepatic gluconeogenesis via dephosphorylation and deacetylation. *Diabetes* **61**, 61–73.

Kitao Y., Ozawa K., Miyazaki M. *et al.* (2001) Expression of the endoplasmic reticulum molecular chaperone (ORP150) rescues hippocampal neurons from glutamate toxicity. *J. Clin. Invest.* **108**, 1439–1450.

Koumura A., Hamanaka J., Shimazawa M., Honda A., Tsuruma K., Uchida Y., Hozumi I., Satoh M., Inuzuka T. and Hara H. (2009) Metallothionein-III knockout mice aggravates the neuronal damage after transient focal cerebral ischemia. *Brain Res.* **1292**, 148–154.

Kudo T., Kanemoto S., Hara H., Morimoto N., Morihara T., Kimura R., Tabira T., Imaizumi K. and Takeda M. (2008) A molecular chaperone inducer protects neurons from ER stress. *Cell Death Differ.* **15**, 364–375.

Kuwabara K., Matsumoto M., Ikeda J. *et al.* (1996) Purification and characterization of a novel stress protein, the150-kDa oxygen-regulated protein (ORP150), from cultured rat astrocytes and its expression in ischemic mouse brain. *J. Biol. Chem.* **271**, 5025–5032.

Lewerenz J. and Maher P. (2009) Basal levels of eIF2alpha phosphorylation determine cellular antioxidant status by regulating ATF4 and xCT expression. *J. Biol. Chem.* **284**, 1106–1115.

Li L., Lundkvist A., Andersson D. *et al.* (2008) Protective role of reactive astrocytes in brain ischemia. *J. Cereb. Blood Flow Metab.* **28**, 468–481.

Morimoto N., Oida Y., Shimazawa M., Miura M., Kudo T., Imaizumi K. and Hara H. (2007) Involvement of endoplasmic reticulum stress after middle cerebral artery occlusion in mice. *Neuroscience* **147**, 957–967.

Mosinger B., Jr, Tillmann U., Westphal H. and Tremblay M. L. (1992) Cloning and characterization of a mouse cDNA encoding a cytoplasmic protein-tyrosine-phosphatase. *Proc. Natl Acad. Sci. USA* **89**, 499–503.

Muppirala M., Gupta V. and Swarup G. (2013) Emerging role of tyrosine phosphatase, TCPTP, in the organelles of the early secretory pathway. *Biochim. Biophys. Acta* **1833**, 1125–1132.

Navis A. C., van den Eijnden M., Schepens J. T., Hooft van Huijsduijnen R., Wesseling P. and Hendriks W. J. (2010) Protein tyrosine phosphatases in glioma biology. *Acta Neuropathol.* **119**, 157–175.

Okada S., Nakamura M., Katoh H. *et al.* (2006) Conditional ablation of Stat3 or Socs3 discloses a dual role for reactive astrocytes after spinal cord injury. *Nat. Med.* **12**, 829–834.

Qi X., Hosoi T., Okuma Y., Kaneko M. and Nomura Y. (2004) Sodium 4-phenylbutyrate protects against cerebral ischemic injury. *Mol. Pharmacol.* **66**, 899–908.

Servidei T., Bhide P. G., Huang Z., Moskowitz M. A., Harsh G. and Reeves S. A. (1998) The protein tyrosine phosphatase SHP-2 is expressed in glial and neuronal progenitor cells, postmitotic neurons and reactive astrocytes. *Neuroscience* **82**, 529–543.

Sofroniew M. V. (2009) Molecular dissection of reactive astrogliosis and glial scar formation. *Trends Neurosci.* **32**, 638–647.

Taguchi A., Soma T., Tanaka H. *et al.* (2004) Administration of CD34 + cells after stroke enhances neurogenesis via angiogenesis in a mouse model. *J. Clin. Invest.* **114**, 330–338.

Tamatani M., Matsuyama T., Yamaguchi A. *et al.* (2001) ORP150 protects against hypoxia/ischemia-induced neuronal death. *Nat. Med.* **7**, 317–323.

Walter P. and Ron D. (2011) The unfolded protein response: from stress pathway to homeostatic regulation. *Science* **334**, 1081–1086.

Yamamoto K., Sato T., Matsui T. *et al.* (2007) Transcriptional induction of mammalian ER quality control proteins is mediated by single or combined action of ATF6alpha and XBP1. *Dev. Cell* **13**, 365–376.

Yeo S., Bandyopadhyay S., Messing A. and Brenner M. (2013) Transgenic analysis of GFAP promoter elements. *Glia* **61**, 1488–1499.

Zabolotny J. M., Bence-Hanulec K. K., Stricker-Krongrad A. *et al.* (2002) PTP1B regulates leptin signal transduction in vivo. *Dev. Cell* **2**, 489–495.

Zamanian J. L., Xu L., Foo L. C., Nouri N., Zhou L., Giffard R. G. and Barres B. A. (2012) Genomic analysis of reactive astrogliosis. *J. Neurosci.* **32**, 6391–6410.